2005 American Control Conference
June 8-10, 2005. Portland, OR, USA

Modeling and Control of a Programmable Filter for Separation of Biologically Active Molecules

Vijay Shilpiekandula and Kamal Youcef-Toumi
Department of Mechanical Engineering
Massachusetts Institute of Technology
Cambridge, MA 02139, USA
Email: svijay@mit.edu, youcef@mit.edu

Abstract— **We present the modeling and control of a programmable filter applicable to the separation of biologically active molecules like proteins and DNA. Conventional methods of separation are bulky, costly and time-intensive. We propose a diaphragm valve design that can filter molecules based on their size by controlling a narrow gap formed between two flat parallel plates. Modeling and experiments performed on a prototype implementation of the gap are presented. Preliminary tests performed on our closed-loop control system indicate that a resolution of 0.2 nm can be achieved for the gap size. Further, to account for any tilt between the plates, we propose the design of a flexure that can compensate for the tilt and ensure the formation of a uniform gap. Dynamic modeling of the flexure and simulations of the tilt-compensation are presented.**

I. Introduction

Filtering biologically active molecules (BAM's), like proteins and DNA, is necessary for the purification and characterization of biological compounds in the pharmaceutical and biotechnology industry. This research focuses on the design and development of a desktop programmable filter for the separation of BAM's. Potential applications of the filter include (i) functioning as a key component of devices that can be developed for the quantification, analysis and diagnosis of body fluids at low costs and faster rates, and (ii) downstream processing of biochemicals in drug discovery [1].

Conventional methods of separation are based on physico-chemical properties like charge, solubility, biological specificity and stereochemistry [2]. These methods are bulky, costly and require the use of additives for enhancing separation. Additional steps are required to recover the biological sample from the additives, resulting in large separation times [3].

In contrast, separation of molecules by size requires no additives and can be applicable over a large range of molecular sizes [2]. Size-based separation techniques hence seem more appropriate in the context of this research.

A size-based separation technique used for our purposes must meet the following requirements [4]: (i) the biochemical composition of the sample must not be altered, (ii) separation of molecules with sizes in the range 0.5-500 nm must be possible, (iii) the technique must be able to distinguish between molecules that vary in size by about 0.1 nm, and (iv) adequate flow rates (10-20 μL/min) of filtered molecules must be achieved.

Implementations of size-based separations, reported recently ([5] and [6]), use an adjustable gap between two flat parallel plates to pass through only particles of size smaller than the gap height. In [5], the gap has been implemented for gas and liquid flow through a 0.2 nm separation of two millimeter-scale polished surfaces. A low-leak MEMS-scale valve for micro-spacecraft missions has been proposed in [6].

Many challenges still need to be addressed in implementing an adjustable gap. The flat plates need to be precisely positioned to ensure that a constant gap size is maintained. To separate molecules that differ in size by as small as 0.1 nm, stringent requirements are placed on the resolution of the positioning mechanism. In implementing such a mechanism for displacements over small (0.5 - 500 nm) ranges, piezoelectric actuators are usually preferred for their high resolution and bandwidth [7]. To achieve a high accuracy in positioning and tracking, the mechanism, with the piezoelectric actuator, needs to be controlled for sufficient bandwidth. The associated control system should be designed to minimize the effects of disturbances such as ambient temperature and pressure fluctuations. Further, effects from non-linearities such as hysteresis and creep in the piezoelectric actuator need to be reduced.

For precise control of the gap, the plates must be parallel to each other to begin with. Any limitations in current manufacturing processes could result in a tilt between the plates, which can not be tolerated for our purpose. Tilt needs to be compensated to ensure the formation of a uniform gap.

The design of a programmable filter addressing the above-stated challenges has been proposed in [4]. Current work is on the implementation of a macro-scale version of this design. Specifically, modeling and control aspects of the adjustable gap and tilt-compensation have been addressed.

The rest of this paper is organized as follows. In Section II, an overview of the design and operation of the filter is presented. We discuss the dynamic modeling of the adjustable gap and the tilt-compensation in Section III. Results of experiments from our prototype implementation of the gap and simulations of tilt-compensation are presented in Section IV. Finally, we summarize current work and present suggestions for future work in Section V.

0-7803-9098-9/05/$25.00 ©2005 AACC

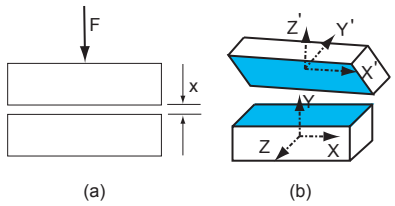

Fig. 1. (a) An adjustable gap x formed between two flat parallel plates is used for size-based separation of BAM's. (b) Due to limitations of fabrication process, the plates can be tilted with respect to each other.

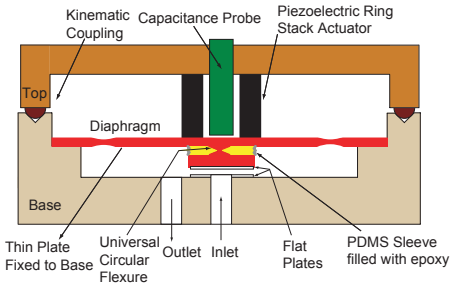

Fig. 2. Conceptual design of our programmable filter [4]. A sectional view of the circular symmetric device is shown.

II. Programmable Filter

A. Overview

Our approach to the separation of BAM's is based on the formation of an adjustable gap between two flat parallel plates. This principle is illustrated in Fig. 1(a). A force F is applied to control the gap size x formed between the plates. Molecules of size smaller than gap size pass through the gap, while the others are filtered out [3].

A conceptual design of the macro-scale version of our filter using this approach is shown in Fig. 2. This design uses a diaphragm valve to achieve the adjustable gap. A piezoelectric ring stack actuator is used to push down on the diaphragm valve. The diaphragm is a monolithic piece consisting of (i) a thin plate fixed on its edges to the base of the device, (ii) a central universal circular flexure, and (iii) a fused silica flat plate (glued to the bottom of the circular flexure) forming the upper boundary of the adjustable gap. The lower boundary of the gap is formed by another flat plate glued to the base. Displacement of the top of the diaphragm is measured with a capacitance probe concentric with the piezoelectric stack in the top housing.

Unlike prior designs ([5] and [6]), this design accounts for modularity. The inner surfaces (of the base and the diaphragm) that confine the flow can be coated with biocompatible materials to ensure that the biochemical composition of the sample remains unaltered during the process of separation. The base and the diaphragm can be replaced, or cleaned and replenished with the coating, while the top housing holding the actuator and sensor can be retained permanently. Further details of the design are provided in [4].

B. Need for Tilt-compensation

The circular flexure in the diaphragm allows for tilt-compensation, the need for which can be explained as follows. Current manufacturing processes do not guarantee that the flat plates are held parallel to each other to begin with. The plates can be randomly oriented in space, as illustrated in Fig. 1(b). To form a uniform gap between the plates, rotary actuators can be used for aligning them precisely along the XYZ axes.

An alternative elegant approach proposed in [3] collapses the two plates onto each other until they mate. In this closed position X', Y', Z' axes of the upper plate are aligned parallel respectively to the X, Y, Z axes of the lower plate. From this position, we open the gap by retracting the upper plate in the Y direction to ensure parallelism with respect to the lower plate, and hence, the formation of a uniform gap between them.

C. Operation

The operation of our device for achieving a precise gap with tilt-compensation is as follows. Initially the piezoelectric actuator is pushed down on the diaphragm till it reaches the base. Upon contacting the base, the bending compliance of the circular flexure allows for the upper plate to tilt and conform to the lower plate. Irrespective of their three-dimensional orientations in space, the plates mate with each other and fully close the gap.

The bending compliance is not desirable, however, when the gap is opened. To account for this, in the next phase of operation, an epoxy is inserted into a polymer sleeve enclosing the circular flexure and allowed to harden. On hardening, the epoxy resists any spring-back arising from the bending compliance of the flexure. Finally, the actuator is retracted to achieve parallel motion of the diaphragm. Closed-loop control of the position of the diaphragm is implemented to achieve the adjustable gap.

III. Modeling

Dynamic modeling of the programmable filter is presented here. Fig. 3 shows a schematic representation of the filter with the piezoelectric actuator, the thin plate and circular flexure, and the flat plates (upper and lower) forming the gap. A lumped parameter model of the filter for analyzing the tilt compensation is presented. The dynamics predicted by lumped parameter model are cross-checked with a finite element model. A model for the transfer function between actuator voltage and diaphragm displacement is fitted to match with the experimental open-loop transfer function of our implementation of the adjustable gap.

A. Lumped Parameter Modeling for Tilt-compensation

A lumped parameter model of the gap formed by the diaphragm and the base is shown in Fig. 4(a). This model is used to analyze the tilt-compensation described in Section II-C. Simulations based on this model will be used to predict the time when tilt-compensation is completed and the epoxy can be inserted.

The thin plate clamped on its edges to the rigid base is modeled as a lumped mass m_1 with a spring k_1 and

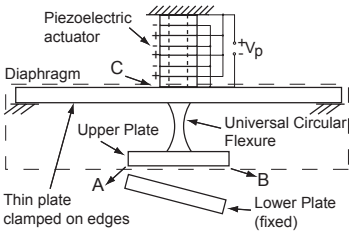

Fig. 3. Schematic representation of the dynamic elements of the programmable filter is shown in (a). Three points of interest in the diaphragm, points A, B and C are shown. These points are defined and their displacements are plotted in Section IV-B for a chosen actuator input.

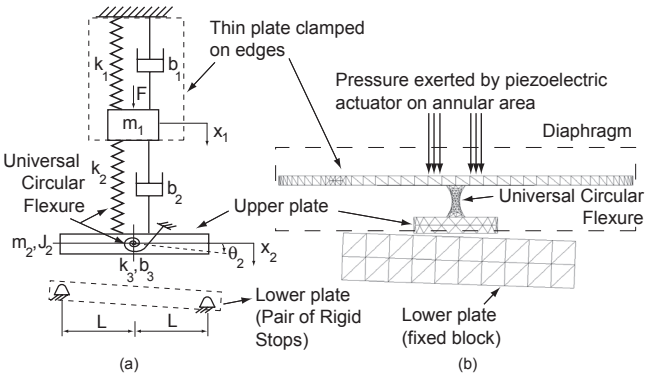

Fig. 4. A lumped parameter model of the filter is shown in (a). A finite element model is shown in (b).

a dashpot b_1 connected to the ground. The upper plate forming the gap is modeled as a lumped mass m_2, with a moment of inertia J_2. The lower plate fixed to the base is modeled as two rigid stops placed at slightly different heights below the upper plate. The universal circular flexure is modeled as consisting of (i) a translational spring k_2 and dashpot b_2 connected between the lumped masses and (ii) a rotational spring k_3 and dashpot b_3 connecting the upper plate to the ground.

The piezoelectric actuator applies a force F on the mass m_1. Initially, this force is increased linearly with time, causing downward motion of the masses m_1 and m_2. At time t_1, the mass m_2 hits the first rigid stop, about which it starts pivoting. The pivoting continues until its impact with the second stop at time t_2. After the tilting action is completed, the force F is kept at a constant value and the epoxy is added. The variation of force F with time is given by:

$$F(t) = At \ \forall \ 0 < t \leq t_F; \quad = At_F \ \forall \ t > t_F \qquad (1)$$

where A is a constant and t_F is any time after the completion of tilt. In analyzing the response of the system to the applied force, we identify three time zones of interest, which are (i) the initial downward motion of the masses - before the onset of any tilt, (ii) the tilting phase when mass m_2 pivots, and (iii) after the completion of tilt.

For a pivoting arm length of L, displacement x_1 (translational) for mass m_1, x_2 (translational) and θ_2 (rotational) for mass m_2, the equations of motion of the masses and the initial conditions (IC's) required for solving them are given below:

$$\text{Before Onset of Tilt}: \ 0 < t < t_{1-}:$$
$$m_1\ddot{x}_1 = F - k_1x_1 - b_1\dot{x}_1 - k_2(x_1 - x_2) - b_2(\dot{x}_1 - \dot{x}_2)$$
$$m_2\ddot{x}_2 = k_2(x_1 - x_2) + b_2(\dot{x}_1 - \dot{x}_2)$$
$$\text{IC}'s: \ x_1(0) = x_2(0) = \dot{x}_1(0) = \dot{x}_2(0) = 0 \qquad (2)$$
$$\text{During Tilting}: \ t_{1+} < t < t_{2-}:$$
$$m_1\ddot{x}_1 = F - k_1x_1 - b_1\dot{x}_1 - k_2(x_1 - x_2) - b_2(\dot{x}_1 - \dot{x}_2)$$
$$m_2\ddot{x}_2 = k_2(x_1 - x_2) + b_2(\dot{x}_1 - \dot{x}_2) - F_R$$
$$F_RL = J_2\ddot{\theta}_2 + b_3\dot{\theta}_2 + k_3; \quad \theta_2(t) = \frac{x_2(t) - x_2(t_{1+})}{L}$$
$$\text{IC}'s: \ x_1(t_{1+}), x_2(t_{1+}), \theta_2(t_{1+})$$
$$\dot{x}_1(t_{1+}), \dot{x}_2(t_{1+}), \dot{\theta}_2(t_{1+}) \qquad (3)$$
$$\text{After completion of tilt}: \ t_{2+} < t < \infty:$$
$$x_2(t) = x_2(t_{2+})$$
$$m_1\ddot{x}_1 = F - k_1x_1 - b_1\dot{x}_1 - k_2(x_1 - x_2) - b_2\dot{x}_1$$
$$\text{IC}'s: \ x_1(t_{1+}), \dot{x}_1(t_{1+}) \qquad (4)$$

The initial conditions for the motion before the onset of tilt are all zero. The initial conditions for the phase of tilting (3) and after completion of tilt (4) need to be derived from models that depict the impact behavior during the infinitesimally small time intervals, $t_{1-} < t < t_{1+}$ and $t_{2-} < t < t_{2+}$ respectively. We derive these initial conditions assuming a perfectly inelastic model for the impacts.

By applying linear and angular momentum principles for the masses, we obtain the following equations of motion during these time intervals, for linear vertical impulses ΔP_1 and ΔP_2 caused due to the impacts:

$$\text{During first impact}: \ t_{1-} < t < t_{1+}:$$
$$x_1(t_{1+}) = x_1(t_{1-}); \quad x_2(t_{1+}) = x_2(t_{1-})$$
$$\dot{x}_1(t_{1+}) = \dot{x}_1(t_{1-}) - \frac{m_2}{m_1}\{\dot{x}_2(t_{1+}) - \dot{x}_2(t_{1-})\} - \frac{\Delta P_1}{m_1}$$
$$\dot{\theta}_2(t_{1+}) = \frac{\Delta P_1 L}{J_2}; \quad \dot{x}_2(t_{1+}) = L\dot{\theta}_2(t_{1+}); \qquad (5)$$
$$\text{During second impact}: \ t_{2-} < t < t_{2+}:$$
$$x_1(t_{2+}) = x_1(t_{2-}); \quad x_2(t_{2+}) = x_2(t_{2-})$$
$$\dot{x}_1(t_{2+}) = \dot{x}_1(t_{2-}) + \frac{m_2}{m_1}\dot{x}_2(t_{2-}) - \frac{\Delta P_2}{m_1}$$
$$\dot{\theta}_2(t_{2+}) = 0; \quad \dot{x}_2(t_{2+}) = 0; \quad \Delta P_2 = \frac{J_2}{L}\dot{\theta}_2(t_{2-}) \qquad (6)$$

The equations of motion (2) – (4) along with the initial conditions specified by (5) and (6) can be solved to obtain the transient response of the system to the applied force.

B. Finite Element Modeling for Tilt-compensation

For the purposes of cross-checking the tilt-compensation predicted by the lumped parameter model of Section III-A, a finite element model of the diaphragm and the base has been generated. The mesh structure generated on ADINA [8] using three-dimensional solid tetrahedral elements is shown

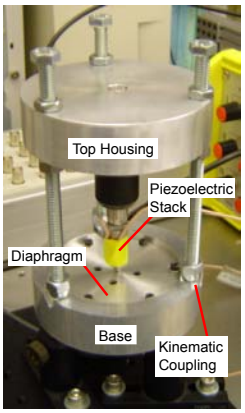

Fig. 5. Photograph of prototype setup for implementing an adjustable gap. A capacitance probe (not shown in figure) fixed to the base senses central deflection of the diaphragm. The stand-off distance for the probe is 100 μm.

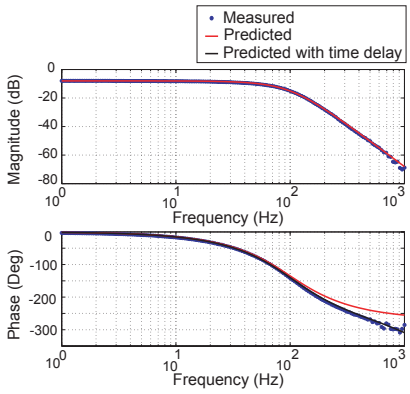

Fig. 6. Experimental and predicted frequency response of the plant transfer function between voltage input to the piezoelectric actuator and the displacement of the diaphragm measured by the capacitance probe.

in Fig. 4(b). The piezoelectric actuator is modeled as a pressure source acting on top of the diaphragm. The geometric boundary conditions applied to this model are (i) edges of the thin plate of the diaphragm are fixed and (ii) the lower plate is fixed.

For simulating tilt-compensation, the pressure applied on the top of the diaphragm was varied as a function of time. The transient response associated with (i) a node on the top of the diaphragm at its center, (ii) the node on the upper plate that first makes the contact with the base, and (iii) the node on the upper plate that last makes the contact are compared with the corresponding responses predicted by the lumped parameter model. These transient responses are presented and compared in Section IV-B.

C. System Transfer Function for Adjustable Gap

A model for transfer function between the diaphragm displacement $Y(s)$ and the actuator voltage $V_p(s)$ is needed to design a control system for the device. We obtained this transfer function by fitting it to match with the experimentally measured frequency response of the transfer function.

Fig. 5 shows a photograph of our prototype experimental setup for achieving an adjustable gap. A Piezomechanik [9] PSt 150/7/20 PZT stack actuator driven by a SVR 150 analog amplifier, set at a gain of 30, pushes down on a 4 inch diameter diaphragm clamped on its edges to a rigid base. A 5 mm diameter ADE [10] 2805 capacitance probe fixed to the base measures the central deflection of the diaphragm. The probe is used with an ADE 3800 gaging system that can be set for a filter cut-off frequency of 100 Hz. With this setting for the filter cut-off frequency, the sensor resolution is specified as 0.15 nm.

A dSPACE DS1103 platform is used at a sample rate of 10 kHz and a resolution of 16 bits per channel for the ADC for PC-based data-acquisition and control of the hardware. A Simulink/dSPACE based dynamic signal analyzer developed by Lilienkamp and Trumper [11], and SigLab [12] were used to capture the experimental frequency response data.

Fig. 6 shows the experimental and predicted frequency response of the open loop system. The system model used to predict the plant transfer function is obtained as follows. The sensor is modeled as a second order lowpass Butterworth filter with a cut-off frequency of 100 Hz. The remaining 40 dB/dec roll-off observed in the frequency range 100-1000 Hz results from the mechanical system, as expected for a piezo-driven positioning mechanism [7]. The phase plot matched well with the experimental data when an additional phase drop from a zero-order hold and full-sample delay [13] due to a dSPACE sample rate of 10 kHz. The overall system transfer function is derived as:

$$\frac{Y(s)}{V_p(s)} = 0.4\left(\frac{3.95\times10^5}{s^2+1005s+3.95\times10^5}\right)\left(\frac{1}{1.6\times10^{-3}+1}\right)\times \frac{(1-e^{-10^{-4}s})}{10^{-4}s}\, e^{-10^{-4}s} \quad (7)$$

IV. Control Implementation, Experiments and Simulations

We are currently testing our diaphragm valve design. In this section, we present results from preliminary experiments performed on our prototype implementation of the adjustable gap. An estimate is needed for the time when epoxy can be inserted as part of operation of the device. Simulations of tilt-compensation based on the lumped parameter and finite element model of the filter are analyzed to obtain this estimate.

A. Adjustable Gap

1) Control System: A control system was built using the Simulink/dSPACE platform for achieving (i) no overshoot and (ii) a 95% settling time of less than 1s. Fig. 7 shows a Simulink model used with MATLAB RTW to develop the dSPACE-based control system. The low pass filter shown in the figure was placed outside the feedback loop (to avoid phase loss) to clean the capacitance probe measurement. To achieve the desired control action, a leadlag compensator was chosen (i) to achieve high DC gain while maintaining

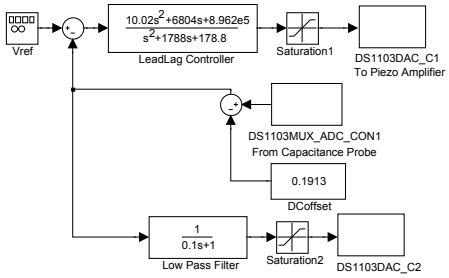

Fig. 7. Simulink Model interfacing with dSPACE controller and plant.

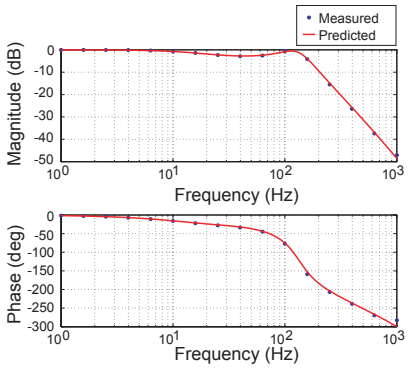

Fig. 8. Experimental and predicted frequency response of the closed-loop transfer function between reference voltage and the displacement of the diaphragm measured by the capacitance probe.

sufficient phase margin and (ii) to limit the noise amplification at frequencies much higher than the crossover. The transfer function of the designed leadlag controller is given by:

$$G_c(s) = \frac{10.02s^2 + 6804s + 8.96\times10^5}{s^2 + 1788s + 178.8} \qquad (8)$$

With this controller, the negative loop transmission has a cross-over frequency of 74.2 Hz and a phase margin of 77.6°. The modeled and experimental frequency response of the closed-loop system transfer function are shown in Fig. 8. The measured closed-loop system -3 dB bandwidth is 150 Hz.

2) Experimental Time Response of Gap: We tested our prototype setup for responses in the time-domain to controlled retraction of the piezoelectric actuator. The step response of the system for a 100 nm peak-to-peak reference signal showed (i) no overshoot, (ii) a 95% settling time of 0.31 s and (iii) a 10-90% rise time of 0.22 s. Further, the system response was recorded for reference staircase signals generated with small (1 nm) incremental steps, each of a 1 s duration. The response to the staircase functions shown in Fig. 9 demonstrates the presence of good tracking of the reference signal by the closed-loop system over a 100 nm range of motion.

3) Resolution of Gap Size: To identify the smallest possible increment of the gap size that can be achieved with our setup, we have recorded the system response to 1 nm, 0.5 nm, and 0.2 nm steps. The system response to 0.2 nm steps is shown in Fig. 10. This response indicates

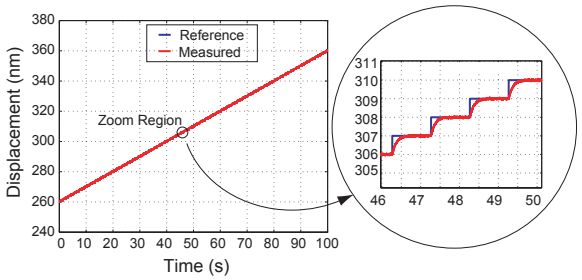

Fig. 9. Displacement over a 100 nm range with incremental 1 nm steps.

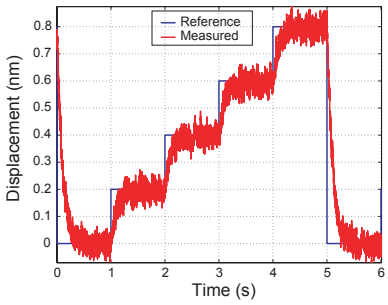

Fig. 10. Measured and reference signals for 0.2 nm steps.

the promise of our current design in achieving high resolutions for gap sizes in the separation of biologically active molecules. The peak-to-peak variation of the noise observed in the response is about 0.1 nm. The presence of this noise introduces a degree of uncertainty in the steady state value of the gap opening achieved with our implementation. We will be characterizing the filter experimentally for its resolution by performing flow tests.

B. Tilt Compensation

Transient dynamics of the diaphragm and the base were simulated to obtain an estimate of the time when tilt-compensation is completed and epoxy can be inserted. A means to monitor the tilt-compensation in real-time is needed. To this end, we consider the transient displacements of select points of the diaphragm indicated in Fig. 1(a). These points are (i) point A in the upper plate that undergoes the first impact with the base and acts as a pivot for the tilting motion, (ii) point B in the upper plate that last comes into contact with the base and (iii) point C on the top of the diaphragm. The displacement of the corresponding points in the lumped parameter model are $x_2(t) - L\theta_2(t)$, $x_2(t) + L\theta_2(t)$ and $x_1(t)$ respectively.

The plots of normalized displacements of the points A, B and C of the diaphragm predicted by the lumped parameter model are shown in Fig. 11. The corresponding normalized displacements predicted by the finite element model are shown in Fig. 12. The forcing function used in these simulations is a ramp until $t = 1$ s and constant thereafter. The response from the lumped parameter and finite element models concur in the trends observed for the normalized displacement data. The displacements have been normalized with respect to the final displacement of point B of the diaphragm. Normalization is done since we are not

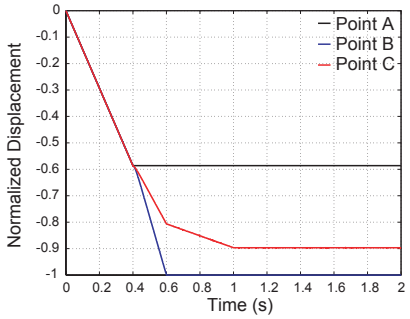

Fig. 11. Normalized displacements corresponding to points A, B and C of the diaphragm (see Fig. 1(a)) obtained from simulations performed on the lumped parameter model. Tilting action is completed at $t \approx 0.6\ s$.

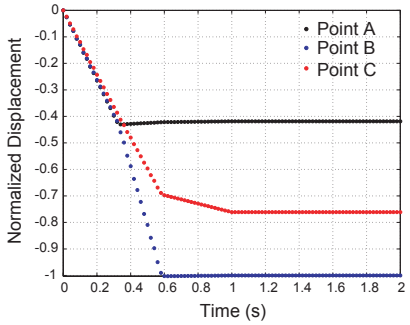

Fig. 12. Normalized nodal displacements corresponding to points A, B and C of the diaphragm (see Fig. 1(a)) obtained from simulations performed on the finite element model.

interested in the exact numerical values, but the variations in slope of the plots.

The trends observed in the graphs of Figs. 11 and 12 can be explained using the lumped parameter model of Fig. 3(b) as follows. Till the first stop is reached, all the points A, B and C have the same deflection. The slope of the displacement graph here is proportional to $1/k_1$. Once the first stop is impacted ($t \approx 0.4\ s$ in the graph of Fig. 11), the point A stops moving (under the assumption of perfectly inelastic impact made in Section III-A) and acts as a pivot for the tilting of mass m_2. The rate at which the point B moves doubles now, since it moves because of both translation and rotation (by the arm length L). Once the tilt-compensation has been fully achieved ($t \approx 0.6\ s$ in the graph of Fig. 11), point B stops moving. This shows up as a change of slope in the displacement of point C on top of the diaphragm. Since the mass m_2 is fixed, the deflection of the mass m_1 is from a parallel combination of springs k_1 and k_2. The slope of the displacement graph for point C hence becomes proportional to $1/(k_1 + k_2)$.

The completion of tilt is indicated by the flattening of the displacement of point B in the diaphragm. Monitoring this displacement should allow us to monitor the tilt-compensation. However, directly sensing the displacement of point B is not feasible. Alternatively, we can sense the change in the slope of the displacement graph of the point C on top of the diaphragm. In our design layout (see Fig. 2), a capacitance probe fixed in the top housing senses the displacement of the top of the diaphragm. With the slope change detected in this measurement, it should be feasible to monitor the tilt-compensation in real-time. Once the completion of tilt-compensation is detected, the actuator force can be kept constant and epoxy added into the PDMS sleeve enclosing the circular flexure.

V. Conclusions

We have examined the concept and operation of our programmable filter applicable to the pharmaceutical and biotechnology industry. Proposed design for an adjustable gap has been modeled and analyzed using a lumped parameter approach. A resolution of 0.2 nm has been achieved for the gap size from preliminary experiments on a prototype macro-scale setup. Tilt-compensation was simulated to obtain an estimate of the time when the epoxy can be added.

We are currently performing more experiments to test and validate our design. Future work will focus on achieving tilt-compensation and biocompatibility of the valve. We are working towards MEMS implementation of our design to achieve separation of biologically active molecules at sufficient flow rates and low filtration times.

VI. Acknowledgements

We would like to thank the Singapore MIT Alliance Program for funding this research. Heejin Choi's assistance with ADINA and Justin Verdirame's assistance with SigLab are acknowledged.

References

[1] Satinder Ahuja, ed. Handbook of Bioseparations. vol. 2. Academic Press, San Diego CA, USA 2000.
[2] Cannell R. Techniques used in Bioproduct Analysis. ch. 5. Butterworth-Heinemann, Boston MA, USA 1992.
[3] Mauricio Gutierrez. Size Adjustable Separation of Biologically Active Molecules. S.M. Thesis, 2004. Department of Mechanical Engineering, Massachusetts Institue of Technology, Cambridge MA, 02139, USA.
[4] Mauricio Gutierrez, Kamal Yocef-Toumi. Programmable Separation of Biologically Active Molecules. Submitted to ICRA 2005.
[5] James R. White. The Nanogate: Nanoscale Flow Control. Doctoral Thesis, 2003. Department of Mechanical Engineering, Massachusetts Institute of Technology, Cambridge MA 02139, USA.
[6] Indrani Chakraborty, William C. Tang, David P. Bame, Tony K. Tang. MEMS Micro-valve for Space Applications. Sensors and Actuators, vol. 83, 2000, pp 188-193.
[7] Han J.M.T.A Anriens, Willem L. de Koning, Reiner Banning. Modeling Piezoelectric Actuators. IEEE Transactions on Mechatronics, vol. 5, no. 4, 2000.
[8] ADINA R&D, Inc. 71 Elton Avenue, Watertown, MA 02472, USA. http://www.adina.com/
[9] Piezomechanik GmBH. Berg am Laim Str. 64 D-81673 Munich, Germany. http://www.piezomechanik.com/
[10] ADE Technologies, Inc. 80 Wilson Way Westwood, MA 02090, USA. http://www.adetech.com/
[11] Katherine A. Lilienkamp, David L. Trumper. Dynamic Signal Analyzer for dSPACE. In Proceedings of the dSPACE User's Conference, May 2000.
[12] SigLab-Dynamic Signal and System Analyzer. Spectral Dynamics, Inc. 1010 Timothy Dr. San Jose, CA 95133. http://www.spectraldynamics.com/
[13] Gene F. Franklin, David J. Powell, Michael Workman. Digital Control of Dynamic Systems. Prentice Hall, 1997.